Establishing a Link Between Amino Acid Sequences and Self-Associating and Viscoelastic Behavior of Two Closely Related Monoclonal Antibodies

Sandeep Yadav • Alavattam Sreedhara • Sonoko Kanai • Jun Liu • Samantha Lien • Henry Lowman • Devendra S. Kalonia • Steven J. Shire

ABSTRACT

Purpose To investigate the underlying cause for the observed differences in self-associating and viscoelastic behavior between two monoclonal antibodies, MAb1, and MAb2.

Methods Several mutants were designed by swapping charged residues in MAb1 with those present in MAb2 at their respective positions and *vice versa*. Rheological analysis was done at low and high shear rates. Dynamic light scattering quantified intermolecular interactions in dilute solutions; sedimentation equilibrium analysis determined the corrected weight average molecular weight (M_{wc}) to assess the self-associating behavior in high concentration. The molecular charge was estimated from electrophoretic mobility measurements.

Results Replacing the charged residues in the CDR of MAb1 resulted in a lower M_{wc} and solution viscosity. The corresponding changes in either just the variable light (VL) or variable heavy (VH) chain showed only a partial decrease in viscosity, whereas changes in both VL and VH chains resulted in a dramatic reduction in viscosity. The converse case where the VL and VH chains of MAb2 were made to look like MAb1 did not self-associate or show increased viscosity.

Conclusions Exposed charged residues in the CDR of MAb1 are critical in determining the self-associating and highly viscous behavior observed at high concentrations.

KEY WORDS high concentration protein solution · intermolecular interactions · protein viscosity/rheology · self-association

S. Yadav · D. S. Kalonia (✉)
Department of Pharmaceutical Sciences
University of Connecticut
Storrs, Connecticut 06269, USA
e-mail: kalonia@uconn.edu

S. Yadav · A. Sreedhara · J. Liu · S. J. Shire (✉)
Late Stage Pharmaceutical Development
Genentech, Inc.
1 DNA Way
South San Francisco, California 94080, USA
e-mail: shire.steve@gene.com

S. Kanai
Pharmaceutical and Analytical R & D
F. Hoffmann La-Roche
Grenzacherstrasse 124
Basel 4070, Switzerland

S. Lien
Antibody Engineering
Genentech, Inc.
1 DNA way
South San Francisco, California 94080, USA

H. Lowman
CytomX Therapeutics, Inc.
460 Ward Drive, Suite E1
Santa Barbara, California 93111, USA

INTRODUCTION

Formulation development of Monoclonal antibodies (MAbs) presents distinct challenges that may not be associated with other therapeutic proteins. MAbs are typically administered in higher doses (~10–200 mg) for the treatment of immunological and allergic disorders or oncology applications. Furthermore, a liquid subcutaneous (SC) formulation is desirable to ensure patient convenience as well as manufacturing ease (1,2). To administer such a high dose with acceptable dose volumes (<1.5 ml) through the SC route, the MAbs need to be formulated over a concentration range from 100 to 200 mg/ml or even higher depending on the indications (2). The high protein

concentration often results in a dramatic increase in the viscosity of the solution (3–6). Thus, high solution viscosity leads to difficulties with pumping, filling, filtering and recovering product from vessels, and can also hamper the injection administration capability of the formulation (1,2,7).

In general, a higher protein concentration shifts the equilibrium towards higher order structures that may favor molecular association or the aggregated state (8–10). The protein associates/aggregates may arise either due to covalent or non-covalent interactions. The generation of covalent aggregate involves a chemical bond formation between monomer species, for instance a disulphide (11) or a bityrosine (12) bond, whereas the non-covalent interactions could be mediated through hydrophobic (13) or electrostatic interactions, such as charge-charge (3,10) or dipole-dipole, (14). The covalent modifications may lead to irreversible aggregates, whereas weak non-covalent interactions generally result in self-associated or reversible aggregates. However, the presence of either of the two may jeopardize the clinical efficacy and long-term stability of the formulation. In addition, the presence of irreversible aggregates may have serious patient safety implications and is known to elicit immunogenic responses (15–18). From a safety and efficacy point of view, self-associated complexes may not be potentially hazardous, if and only if the self-associated forms are completely reversible upon dilution prior to administration (19). However, if the dissociation rate is slow as compared to the *in vivo* clearance rate, the complexes may lead to increased exposure or even elicit an immunogenic response on SC administration (19). Furthermore, self-associated forms may act as precursors and impact the rate of irreversible aggregate formation through generation of covalent linkages during storage (20).

The MAb formulations, therefore, need to be optimized for the viscosity as well as self-association and aggregation, both of which represent the most critical consequence of developing a high concentration formulation.

MAb1 (IgG$_1$; M$_w$≈145 kD) represents one such molecule wherein high concentration results in both self-association and a dramatic increase in solution viscosity (3). There has been considerable effort lately in understanding the self-associating and viscosity behavior of MAb1 (3,21,22).

Liu *et al.* showed that the reversible self-association of MAb1 molecules at high concentrations correlated with the observed high solution viscosity (3). At low ionic strengths (15 mM), the viscosity was highest at pH 6.0 and decreased rather sharply as the solution pH was changed to either the acidic or the basic side of pH 6.0. Sedimentation equilibrium analysis suggested that MAb1 tends to self-associate weakly and reversibly at high concentration. The addition of 150 mM salt (NaCl) resulted in a considerable drop in viscosity as well as lower corrected M$_w$ of MAb1. This result clearly implicated electrostatic interactions in governing the self-associating and viscosity behavior of MAb1 (3).

Later, Kanai *et al.* proposed that the self-association in MAb1, at pH 6.0, originates from multiple Fab-Fab interactions (21). The authors compared the viscosity behavior of full-length as well as Fab and F(ab′)$_2$ fragments of MAb1 and MAb2 molecules. At high concentrations the full length MAb1 showed a much higher viscosity as compared with MAb2 solutions. The solution of F(ab′)$_2$ fragments of MAb1 also showed a higher viscosity as compared with MAb2 F(ab′)$_2$ fragments, indicating the network interaction leading to self-association remains intact in MAb1 even without the Fc domain. The loss of solution viscosity of MAb1 F(ab′)$_2$ fragments with addition of salt corroborated that the interactions originated specifically from Fab regions and were electrostatic in nature (21).

Further, Yadav *et al.* showed that the presence of specific attractive interactions at pH 6.0 leads to the self-association and high viscosity of MAb1 at high concentrations (22). The authors quantified the net charge and the intermolecular interactions as a function of solution pH and ionic strength in both dilute and high concentration MAb1 solutions. The observed pH-dependent viscosity behavior for MAb1 correlated well with the nature of intermolecular interactions at various solution conditions. At pH 6.0, strong attractive interactions, conducive to self-association and high viscosity, persisted in MAb1 solutions despite a net positive charge on the molecule. These intermolecular attractions originated specifically from the Fab regions due to the presence of a number of charged residues, especially histidyls, in the complementarity-determining regions (CDR) (22). In subsequent work, the authors employed the modified Ross and Minton equation to demonstrate that the presence of intermolecular attractions led to an increase in the effective volume of MAb1 (labeled as MAb-A) at high concentrations, demonstrating the self-association of MAb1 at pH 6.0 (6).

The present investigation was intended primarily to identify and confirm the role of specific charged residues, present in the CDR, towards the self-associating and high viscosity behavior of MAb1. The study concentrates on the solution behavior of several charge-swap mutants obtained by performing mutations in the variable light (VL) and variable heavy (VH) chains of MAb1 and in another monoclonal antibody, MAb2, which does not show significant self-association or high viscosity at high concentration (>100 mg/mL) at pH 6.0.

MATERIALS AND METHODS

Materials

Monoclonal Antibodies and Designed Mutants

The monoclonal antibodies MAb1, MAb2, M-1, M-5, M-6, M-7, M-10 and M-11 were produced at Genentech Inc. (South San Francisco, CA). The antibodies, MAb1 and MAb2, were constructed with essentially the same human IgG$_1$ framework, with κ light chain, and the major differences reside in the complementarity-determining regions (CDR) and flanking amino acid residues. MAb1 was the same MAb referred to as MAb1 by Liu et al. (3) Kanai et al. (21) and Yadav et al. (22), and MAb2 was the same MAb referred to as MAb2 by Liu et al. (3).

Description of Mutants

MAb1 and MAb2, as stated previously, were constructed from the same IgG$_1$ human Fc framework. Thus, the differences between the two IgG$_1$s reside in the CDRs. In addition to specific site amino acid differences (discussed below), there is also a 4 amino acid insert (SVDY) in the CDR1 light chain of MAb1. In order to ascertain if this additional sequence had any impact on the viscosity properties of MAb1, the mutant M-1 was created with the 4 amino acid insert removed. It should also be noted that slight heterogeneity of the carbohydrate is common during CHO production (23). To determine whether the carbohydrate played a major role in viscosity of these antibodies, MAb1 was expressed and purified from E. coli to produce the aglycosylated version of MAb1, designated as M-11.

To understand the self-associating behavior of MAb1 (originating from Fab regions) (21,22), the amino acid sequence in the CDR of MAb1 was compared with the sequence of MAb2, which does not self-associate to nearly the same extent as MAb1 at pH 6.0, and low ionic strength. It was observed that a number of charged residues are present in the sequence of MAb1, both in the variable light (VL) and variable heavy (VH) chain, which are absent in the sequence of MAb2 at the respective positions. The charged residues present in the VL chain include some aspartates, glutamates and histidyl residues, whereas the VH chain consists of a number of histidyl residues. To elucidate whether these charged residues are responsible for self-association at high concentration, several mutants were designed by swapping charged residues in MAb1 with those present in MAb2 at their respective positions, and vice versa.

M-5, M-6 and M-7 represent mutations made in the sequence of MAb1, whereas M-10 is the MAb2 mutant. M-5 and M-6 are the mutants where the mutations were made only in the VL or the VH chains, respectively. In the case of M-7, the charged residues in both the VL and VH chains were swapped. M-10 represents a mutant where the charged residues present in the sequence of MAb1 were substituted in both the VL and VH chain sequence of MAb2. A description of the different mutants used in this study has been summarized in Table I.

The aim of designing these mutants was to minimize the sequence variation between two molecules, i.e. MAb1 and MAb2, and determine whether one behaves like the other with respect to viscosity and self-associating behavior. Studies on the viscosity and intermolecular interaction behavior of M-5, M-6 and M-7 will, therefore, help in determining whether the specific interactions originate exclusively from the VL chain or the VH chain, or if the presence of charged residues on both VL and VH are responsible. M-10 was constructed to allow us to determine the contribution of factors in addition to charged residues, to the self-associating behavior.

Table I Description of Mutants Designed by Performing Mutations in the CDR Sequence of MAb1 or MAb2

CDR:	Light Chain 1[a]	Light Chain 3[a]	Heavy Chain 3[b]	The rest of the CDR	Description
MAb1	QSV**D**Y**D**G**D**SYMN	**HED**PYT	GS**H**YFG**H**W**H**FAVW	MAb1 LC & HC	MAb1 WT
MAb2	Q——**D**V**N**TAVA	**Y**TTPPT	WG**GD**GF**YAMD**YW	MAb2 LC & HC	MAb2 WT
M-1	Q——**D**G**D**SYMN	**HED**PYT	GS**H**YFG**H**W**H**FAVW	MAb1 LC & HC	MAb1 with SVDY deletion in LC1
M-5	QSV**D**YA**GN**SYMN	**Y**TTPYT	GS**H**YFG**H**W**H**FAVW	MAb1 LC & HC	MAb1 with substitution in LC1 and LC3
M-6	QSV**D**Y**D**G**D**SYMN	**HED**PYT	GS**G**YFG**Y**W**M**FAVW	MAb1 LC & HC	MAb1 with substitution in HC3
M-7	QSV**D**YA**GN**SYMN	**Y**TTPYT	GS**G**YFG**Y**W**M**FAVW	MAb1 LC & HC	MAb1 with substitution in LC1, LC3 and HC3
M-10	**E**——**D**V**D**TAVA	**HED**PPT	WG**HD**GF**HA**H**D**YW	MAb2 LC & HC	MAb2 with substitution in LC1, LC3 and HC3
M-11	QSV**D**Y**D**G**D**SYMN	**HED**PYT	GS**H**YFG**H**W**H**FAVW	MAb1 LC & HC; made in E. Coli.	Aglycosylated MAb1

Mutations performed in the variable light (VL)[a] and variable heavy (VH)[b] chain sequence. Numbers 1, and 3 correspond to the different loops of the variable regions (LC light chain; HC heavy chain) in the CDR.

Reagents and Chemicals

Acetic acid, sodium acetate, sodium chloride, histidine hydrochloride, monobasic and dibasic sodium phosphate, tris (hydroxymethyl) aminomethane, sodium hydroxide and hydrochloric acid were obtained from Fisher Scientific (Fair Lawn, NJ, USA). All chemicals used were reagent grade or higher. Deionized water equivalent to Milli-Q™ grade was used to prepare all solutions. Millipore (Billerica, MA) Amicon Ultra centrifugation tubes with a molecular weight cut-off of 10 kD were obtained from Fisher Scientific. Quartz crystal discs, with fundamental vibrating frequencies of 10 MHz and plated with gold electrodes on both sides were obtained from International Crystal Manufacturing Company (Oklahoma City, Oklahoma). Fluorocarbon (FC-43) was obtained from Beckman Instruments (Palo Alto, CA).

Analytical Methods

Sample Preparation

Acetic acid-sodium acetate (pH 4.0, 5.0), histidine hydrochloride (pH 6.0), monobasic-dibasic sodium phosphate (pH 7.0 and 8.0), and N,N-Bis(2-hydroxyethyl)glycine (Bicine) (pH 9.0) buffers were prepared to maintain the solution pH. Appropriate buffer concentrations were selected to maintain the ionic strength at 15 mM without the addition of any salt. For high ionic strength studies, sodium chloride was added to adjust the total solution ionic strength to 150 mM. Prior to analysis, the antibody solutions were buffer exchanged with the buffer of interest using Millipore Amicon Ultra centrifugation tubes with a molecular weight cut-off of 10 kD. After buffer exchange, the concentrations of the samples were determined using a UV spectrophotometer and an absorptivity of 1.6 $(mg/mL)^{-1}cm^{-1}$ for MAb1, M-1, M-5, M-6, M-7, M-11, and 1.5 $(mg/mL)^{-1} cm^{-1}$ for MAb2 and M-10 at 280 nm for 0.1% IgG_1 solutions. The solution pH was checked for each dialyzed sample. Required concentrations were prepared by dilution with the respective buffer.

Circular Dichroism Measurements

Near-UV circular dichroism (CD) spectroscopy was used to ensure that no major structural change resulted in the tertiary structure of MAbs upon mutations of different residues. Experiments were conducted using a Jasco 815 spectropolarimeter (Easton, MD, USA). Solution ellipticity was measured from 340 to 240 nm at pH 6.0 histidine-HCl buffer. Studies were conducted at 0.75 mg/ml MAb concentration using a 10 mm path length cell. Multiple scans, at a resolution of 0.1 nm and a scan rate of 10 nm/min, were accumulated and averaged in order to improve the signal-to-noise ratio. Buffer spectra obtained with the same acquisition parameters were subtracted from the averaged scans for the IgG_1 solutions.

Viscosity Measurements

Viscosities of samples were measured with an MCR300 cone and plate rheometer (Anton Paar, Ashland, VA). Samples were loaded onto the lower measuring plate and were allowed to come to thermal equilibrium at 25°C. A solvent trap was used to prevent solvent evaporation. The samples were subjected to two cycles of shear-rate sweeps with a 1-min resting time between the two cycles. The shear rate was ramped up from 10 to 1,000 s^{-1} with a 1-min hold time at 1,000 s^{-1} and then ramped down from 1,000 to 10 s^{-1}. Due to the shear thinning behavior of protein solutions the viscosity values reported are at 1,000 s^{-1} owing to the shear rate independence of viscosity at this frequency. The reported values are an average of two shear-rate sweep measurements. The duration of measurement at each shear rate was optimized using the US200 software (Anton Paar, Ashland, VA).

Sedimentation Equilibrium Studies

Sedimentation Equilibration analyses of IgG_1 molecules were conducted using a Beckman XL-1 ultracentrifuge at 20°C, using the preparative method described previously (3, 24, 25). The method was optimized for the IgG_1 loading concentration, loading volume, sedimentation equilibrium attainment time and speed (RPM). Approximately 300 µl of IgG_1 solutions were layered on top of 100 ml of Fluorocarbon (FC-43) in thick-walled polycarbonate tubes (Beckman Instruments, Palo Alto, CA). The samples were than centrifuged for 12,000/15,000 rpm in a swinging bucket SW 60 Ti rotor for 36–48 h. Sample loading concentrations of 50 mg/ml and volumes of 300 µl were enough to acquire a good number (average 12–15 points) of data points. Sedimentation equilibrium was attained within 48 h at 12,000 rpm. Attainment of sedimentation equilibrium was verified by comparing data obtained after centrifugation for 48 and 64 h. Immediately after centrifugation, aliquots (10 µl fractions) of the sample were withdrawn using a BRANDEL® automated micro-fractionator (minimum step size: 5 mm). The collected fractions were placed into a 96-well UV plate and diluted with 30 mM histidine-HCl buffer for measuring protein concentration by UV spectroscopy.

The apparent weight average molecular weight, $M_{w,app}$, at each radial position was determined with the following equation (24):

$$C_r = C_0 e^{\frac{M_{w,app}.\omega^2.(1-v\rho).(r^2-r_0^2)}{2.R.T}} \tag{1}$$

where C_r is the IgG$_1$ concentration at the radial position r, C_o is the initial loading protein concentration, v is the partial specific volume, ρ is the buffer density, ω is the angular velocity, r_o is the reference radial position, R is the gas constant, and T is the temperature in degrees Kelvin. The values for the partial specific volumes, v, for MAb1 (0.73 ml/g), MAb2 (0.72 ml/g), M-7 (0.73 ml/g) and M-10 (0.72 ml/g) were calculated from their amino acid and carbohydrate compositions using the program SEDNTERP (www.bbri.org/RASMB/rasmb.html). The buffer density, ρ (1.011 g/ml) for histidine-HCl, 15 mM ionic strength at pH 6, was determined using a digital densitometer (DMA35, Parr, Paar, Ashland, VA). The apparent weight average molecular weight as a function of protein concentration for each MAb molecule was obtained from a sliding regression of the slope of the natural logarithm of protein concentration, *vs.* radial position. (ln c *vs.* $r^2/2$ plot). Thermodynamic non-ideality at high concentrations due to the primary charge effect and excluded volume results in an apparent weight average molecular weight less than the monomer molecular weight of a typical IgG$_1$ molecule [26–28].

The non-ideality corrections for the charge and excluded volume can be obtained, assuming MAb2 exists as monomeric species ($M_w = 150$ kD) and does not self-associate appreciably in solution. These corrections can be obtained from the following relationship between $M_{w,app}$ at weight/volume concentration, c, and the actual molecular weight, M_w [29,30]:

$$M_{w,app} = M_w\left[1 + c\left(\frac{d\ln\gamma}{dc}\right)\right] = 150,000*(Corr(c)) \qquad (2)$$

where, γ is the activity coefficient of IgG$_1$ molecule and $Corr(c)$ is the multiplicative correction factor.

High Frequency Ultrasonic Rheology

The rheological properties of the monoclonal antibodies were evaluated using an ultrasonic shear rheometer with quartz crystals vibrating at a fundamental frequency of 10 MHz. The theory and experimental procedure have been described elsewhere [31]. For non-Newtonian viscoelastic fluids, the solution storage (G′) and loss (G″) moduli and the complex viscosity (η*) are given by the following relationships [31, 32]:

$$G'(\omega) = \frac{R_2^2 - X_2^2}{A^2 \rho_{Liq.}}, \qquad (3)$$

$$G''(\omega) = \frac{2R_2 X_2}{A^2 \rho_{Liq}} \qquad (4)$$

$$\eta^* = ((G')^2 + (G'')^2)^{1/2}/\omega = G^*/\omega \qquad (5)$$

where A is a crystal constant, ρ_{Liq} is the liquid density, and ω is the quartz crystal frequency. In this study, 35-μL samples of the IgG$_1$ solution were analyzed in triplicate. The temperature of the liquid samples was controlled at 25 ± 0.1°C prior to and during measurement using a temperature-controlled water jacket.

Dynamic Light Scattering (DLS)

DLS studies were conducted at 25 ± 0.1°C using a Malvern Zetasizer Nano Series (Worcestershire, UK). The buffers were filtered through sterile 0.22 μm Durapore membrane filters (Millipore, Bellirica, MA) before centrifugal ultrafiltration. After buffer exchange, the protein solutions were filtered through 0.22 μm Millex-W syringe filters (Millipore). The concentration of IgG$_1$ in the solution was adjusted to 12 mg/ml, and the pH was measured to ensure consistency. Before analysis, the protein solutions were centrifuged at $6,740\times g$ for 5 min using an eppendorf minispin (Germany HA) centrifuge. A low volume glass cuvette, DTS2145 (Malvern Instruments, UK), was used for holding the sample. A total of 15 scans, each with duration of 20 s, were accumulated for each sample. All the samples were analyzed in triplicate. DTS software (Malvern Instruments, UK) was used to analyze the acquired correlogram (correlation function *versus* time) and obtain the mutual diffusion coefficient (D_m). The hydrodynamic radius (R_h) of the molecules can be estimated from the D_s using the Stokes-Einstein equation, $D_s = k_B T/6\pi\eta R_h$, where k_B is the Boltzmann constant, T is the temperature in degrees Kelvin and η is the solvent viscosity, i.e. $c \rightarrow 0$.

Zeta Potential and Net Charge Determination

Zeta potential (ξ) measurements were performed at 25 ± 0.1°C essentially as described previously [6] using a Malvern Zetasizer Nano Series (Worcestershire, UK). For the convenience of the reader the procedure is briefly described again. The measurements were made using an antibody concentration of 5 mg/ml in a DTS1060 clear disposable folded capillary cell. The electrophoretic mobility measured under an applied electric field is then used to determine the zeta potential using Henry's equation:

$$U_E = \frac{2\varepsilon\xi f_1(\kappa a)}{3\eta} \qquad (6)$$

where U_E is the electrophoretic mobility under the applied voltage, ε is the dielectric constant of the medium, η is the viscosity of the dispersant, ξ is the zeta potential in Volts and $f_1(\kappa a)$ is the Henry's function. Different solutions exist for $f_1(\kappa a)$ depending upon the ratio of the radius of curvature to the thickness of the electrical double layer around the

particle (33,34). At 15 mM solution ionic strength, the $f_1(\kappa a)$ value of 1.066 was used to calculate the zeta potential.

If the zeta potential of a particle is less than kT/e (i.e. 25.7 mV at 25°C), the net molecular charge can be approximated using the Debye-Hückel approximation of the Poisson-Boltzmann equation:

$$z = \frac{4\pi\varepsilon a(1 + \kappa a)\xi}{e} \qquad (7)$$

where e is the electronic charge, a is the particle radius and the inverse Debye length κ is given by (35).

$$\kappa = \left(\frac{8\pi N_o e^2}{1000\varepsilon kT}\right)^{1/2} I^{1/2} \qquad (8)$$

where N_o is Avogadro's number and k is Boltzman's constant, I is the solution ionic strength and T is the temperature in degrees Kelvin. For the present charge calculations, the radius a has been substituted by the hydrodynamic radius, R_h calculated using the Stokes-Einstein equation from the self-diffusion coefficients, D_s, obtained from DLS measurements. The use of the exclusion/hydrodynamic radius, R_h, over the van der Waals radii a is justified because it is the Stokes radius that defines the size of an electro-hydrodynamic particle (36,37).

Theoretical Charge Calculations

The theoretical charges on different IgG$_1$ molecules were calculated using the primary amino acid sequence. The charges were calculated as function of solution pH using SEDNTERP. (www.bbri.org/RASMB/rasmb.html).

RESULTS

Impact of Amino Acid Sequence Insert and Glycosylation on Viscosity of MAb1

The viscosity as a function of concentration for mutant M-1 is similar to the respective parent IgG$_1$ molecule, MAb1 (Fig. 1). These data show that the absence of the 4 amino acid sequence in the CDR of MAb1does not have a major effect on the viscoelastic properties of this monoclonal antibody. In addition, mutant M-11, which was produced in *E. coli*, has a similar viscosity-concentration profile when compared to the glycosylated version, MAb1 (Fig. 1).

Viscosity *vs.* Concentration for MAb1, MAb2 and Their Respective Charge-Swap Mutants

Mutants with substitution of charged residues, only in the VL chain (M-5) or in the VH chain (M-6) showed a partial loss in
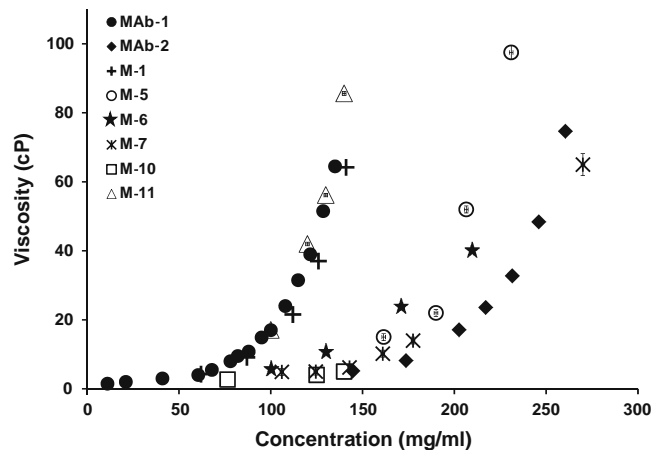
Fig. 1 Viscosity profile of MAb1, Mab2 and the designed mutants as a function of concentration at solution pH 6.0, 15 mM ionic strength. The viscosity was measured with MCR300 rheometer (Anton PAAR), using a CP25-1 cone/plate measuring system at a shear rate of 1,000/s.

viscosity, but the viscosity values are still higher than that observed for MAb2 (Fig. 1). On the other hand, viscosity of M-7, with charge changes in both VL and VH chain, is equivalent to MAb2 (Fig. 1). Interestingly, M-10, where charge residues from MAb1 are substituted in the sequence of MAb2, did not show any increase in the viscosity (Fig. 1).

High Frequency Rheology of MAb1, MAb2 and Charge-Swap Mutants M-7 and M-10

Figure 2a shows the solution G′ as a function of IgG$_1$ concentration for MAb1, MAb2, and the charge-swap mutants, M-7 and M-10, at solution pH 6.0, 15 mM ionic strength. MAb1 showed a high solution G′ at high concentrations and a sharp increase with concentration, whereas M-7 did not show such high solution G′ at 125 mg/ml. The solution G′ for MAb2 and M-10 at 125 mg/ml was also significantly less in comparison to MAb1 along with a gradual increase with concentration. The solution G′, as a function of pH for these molecules at 125 mg/ml, is shown in Fig. 2b. MAb1 showed a monotonic decrease of G′ with an increase in pH from 6.0 to 8.0, whereas M-7 did not show any significant change in G′ on changing solution pH from 6.0 to 7.0, though the G′ increased with a further rise in solution pH to 8.0 (Fig. 2b). Both MAb2 and M-10 showed an increase in solution G′ with increasing solution pH, wherein solution pH 8.0 showed the highest G′ (Fig. 2b). In addition, at pH 8.0 MAb2 showed a higher G′ in comparison to M-10 (Fig. 2b).

Dynamic Light Scattering Studies of MAb1, MAb2, and Charge-Swap Mutants M-7 and M-10

Figure 3a and b show the results from the DLS measurements. Figure 3a shows a representative plot at pH 6.0,
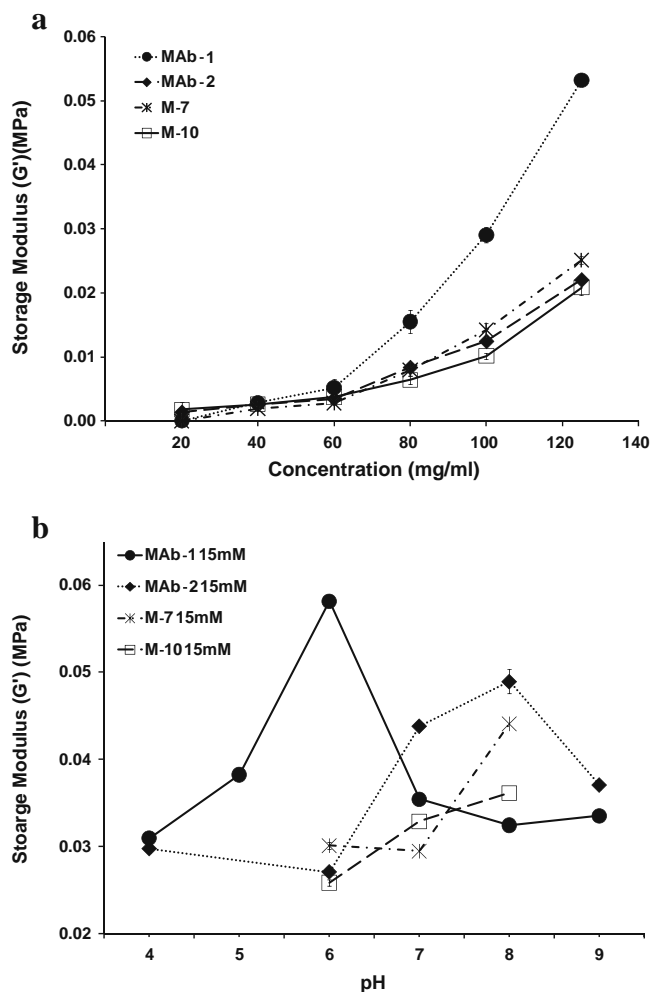
Fig. 2 Solution storage modulus (G′) measured using ultrasonic shear rheometer at 10 MHz frequency (**a**) as a function of IgG₁ concentration at pH 6.0, 15 mM ionic strength (**b**) as a function of solution pH at 125 mg/ml. The measurements were made in triplicate. The *error bars*, if not visible, are smaller than the symbols used. The line connects the data points to guide the eye and is not a result of model fitting to the data. The G′ data only for MAb1 has been published previously in Reference 22.

from a positive to a negative value. Previous DLS measurements on MAb1 at pH 6.0, 15 mM ionic strength resulted in a k_D of −21.05 ml/g (22) and −18.54±0.53 ml/g (6). The k_D value reported in this work (−19.79±1.11 ml/g) is an average of the earlier two reported values as well as some additional measurements (6,22). The measurements are usually repeated with every new lot of MAb1 received, and essentially represent 5–6 replicates over time for MAb1. However, the associated experimental error does not change any conclusion or interpretation of either this work or any of the previously published manuscripts (6,22).

The interaction parameter, k_D, as a function of pH is shown in Fig. 3b. The value of k_D for MAb1 becomes less negative as the solution pH is increased from 6.0 to 8.0 (Fig. 3b). At pH 9.0 the k_D attains a positive magnitude,
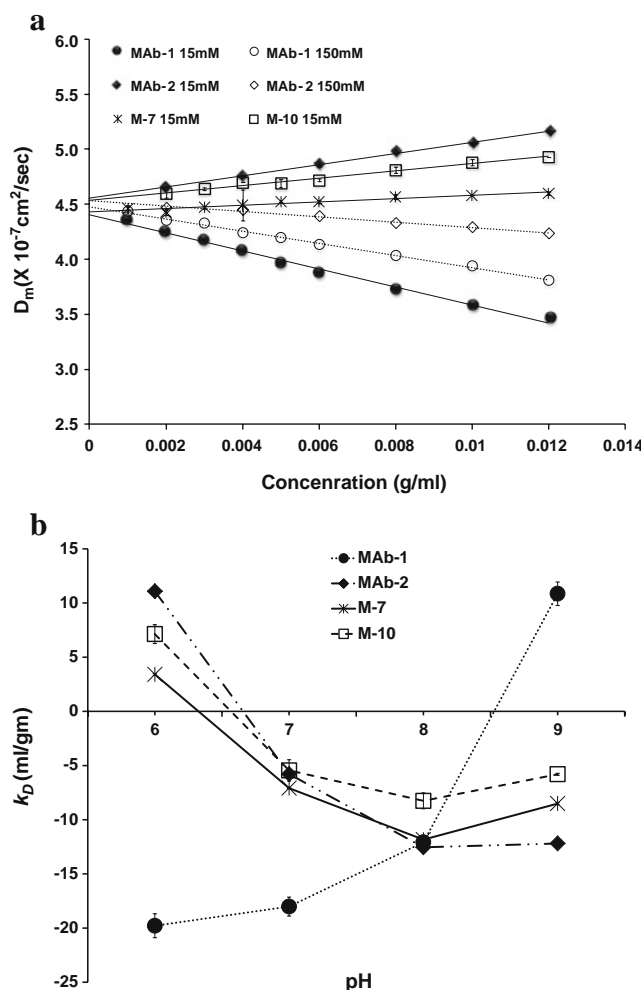

Fig. 3 (**a**) Mutual diffusion coefficient (D_m) for IgG₁ molecules at pH 6.0, 15 mM (*solid symbols*) and 150 mM (*open symbols*) solution ionic strength. The ionic strength was adjusted to 150 mM with addition of NaCl. The lines are linear best fits with slope and intercept representing $D_s k_D$ and D_s (self diffusion coefficient), respectively. (**b**) The interaction parameter, k_D, as a function of solution pH, calculated from the slopes of D_m versus c plots (Eq. 9).

where the mutual diffusion coefficients (D_m) are plotted as a function of IgG₁ concentration ranging from 3 to 12 mg/ml. The lines in the figure represent linear fits to the data using the following equation (38,39):

$$D_m = D_s(1 + k_D c) \qquad (9)$$

where D_s is the self-diffusion coefficient (the value of D_m at c =0), k_D is the interaction parameter, and c is the concentration of the protein (g/ml). The value of D_s and k_D can be obtained, respectively, from the intercept and slope of a plot of D_m *vs*. c (Eq. 9). The parameters Table II) at pH 6.0, 15 mM ionic strength, for MAb1 and M-6 showed a negative k_D, whereas MAb2, M-5, M-7 and M-10 have a positive k_D. At 150 mM solution ionic strength, MAb1 showed a less negative k_D, whereas the k_D for MAb2 changed

Table II Parameters Calculated From DLS Measurements With IgG_1 Molecules at $25 \pm 0.1°C$

pH	$D_s \times 10^{-7}$ (cm²/sec)[a]	d_H (nm)[b]	k_D (ml/gm)[c]
MAb1, 15 mM ionic strength			
6.0	4.27 ± 0.05	11.48 ± 0.18	-19.79 ± 1.11
7.0	4.34 ± 0.08	11.30 ± 0.28	-18.02 ± 0.88
8.0	4.24 ± 0.04	11.51 ± 0.14	-12.08 ± 0.05
9.0	4.17 ± 0.09	11.77 ± 0.32	$+10.86 \pm 1.09$
MAb1, 150 mM ionic strength			
6.0	4.48 ± 0.03	10.96 ± 0.11	-12.32 ± 0.48
MAb2, 15 mM ionic strength			
6.0	4.32 ± 0.03	10.77 ± 0.11	11.09 ± 0.07
7.0	4.56 ± 0.07	10.79 ± 0.25	-5.79 ± 0.23
8.0	4.55 ± 0.06	10.82 ± 0.21	-12.55 ± 0.08
9.0	4.52 ± 0.06	10.86 ± 0.21	-12.19 ± 0.16
MAb2, 150 mM ionic strength			
6.0	4.53 ± 0.04	10.83 ± 0.14	-5.38 ± 0.64
M-5, 15 mM ionic strength			
6.0	4.43 ± 0.03	10.99 ± 0.11	8.04 ± 0.66
M-6, 15 mM ionic strength			
6.0	4.32 ± 0.06	10.77 ± 0.21	-14.22 ± 1.20
M-7, 15 mM ionic strength			
6.0	4.43 ± 0.03	10.99 ± 0.11	10.66 ± 0.04
7.0	4.48 ± 0.01	10.95 ± 0.04	10.62 ± 0.07
8.0	4.46 ± 0.02	10.95 ± 0.07	10.77 ± 0.05
9.0	3.97 ± 0.08	12.35 ± 0.28	-8.51 ± 0.11
M-10, 15 mM ionic strength			
6.0	4.54 ± 0.06	10.66 ± 0.20	7.13 ± 0.87
7.0	4.54 ± 0.08	10.62 ± 0.27	-5.45 ± 0.99
8.0	4.53 ± 0.02	10.77 ± 0.08	-8.26 ± 0.74
9.0	4.44 ± 0.07	11.06 ± 0.25	-5.80 ± 0.09

[a] From the intercept of plots in Fig. 3(a)

[b] True Hydrodynamic diameter calculated at $c \rightarrow 0$

[c] Slope (plots in Fig. 3(a))/D_s

whereas the values for MAb2, M-7 and M-10 are positive at pH 6.0 and become negative at pH 9.0 (Fig. 3b).

Circular Dichroism Studies

Figure 4a shows the near UV CD spectra for MAb1 and M-7 where the charged residues have been replaced in both the VH and VL chain sequences. The ellipticity is represented as mean residue molar ellipticity. Although there are subtle differences in the near UV CD spectra for MAb1 and M-7, no major change in the structure of M-7 is observed. Moreover, the observed differences in mean residue molar ellipticity of MAb1 and M-7 are expected due to the substitution of different residues upon mutation. In comparison to the charged residues present in the sequence of MAb1, MAb2 possesses certain aromatic

(tyrosine) residues at the respective position and some tryptophan residue in the vicinity. Therefore, swapping of charge residues in MAb1 with those present in MAb2 at their respective positions results in the insertion of some aromatic residues in the sequence of M-7. This is reflected as increased molar ellipticity in the case of M-7 in comparison to MAb1. Similarly, no major change was observed in the CD spectra for M-10 in comparison to MAb2 (Fig. 4b), indicating that the overall structure of IgG_1 molecules remains intact following mutation.

Analytical Ultracentrifugation Studies

Figure 5a shows the concentration gradient generated by preparative analytical ultracentrifugation for the different IgG_1 molecules as a function of centrifugal radial position. Among all IgG_1 molecules, MAb1 with the highest viscosity showed the steepest concentration gradient. The apparent
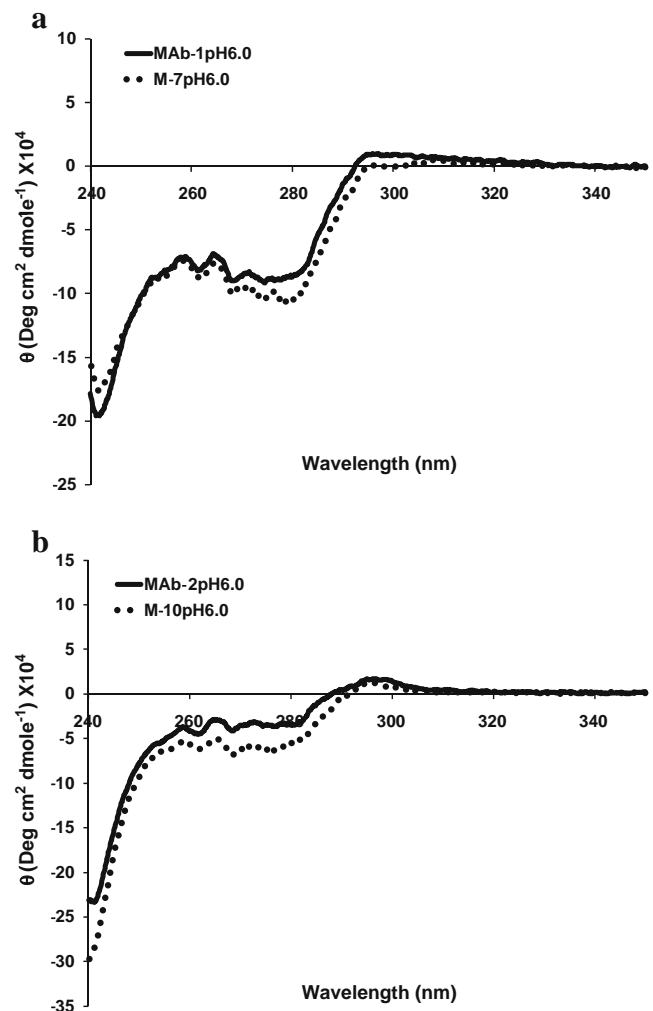
Fig. 4 Near UV CD spectra of (**a**) MAb1 and M-7 and (**b**) MAb2 and M-10 at solution pH 6.0, histidine hydrochloride buffer at 15 mM ionic strength. The ellipticity is represented as mean residue molar ellipticity.
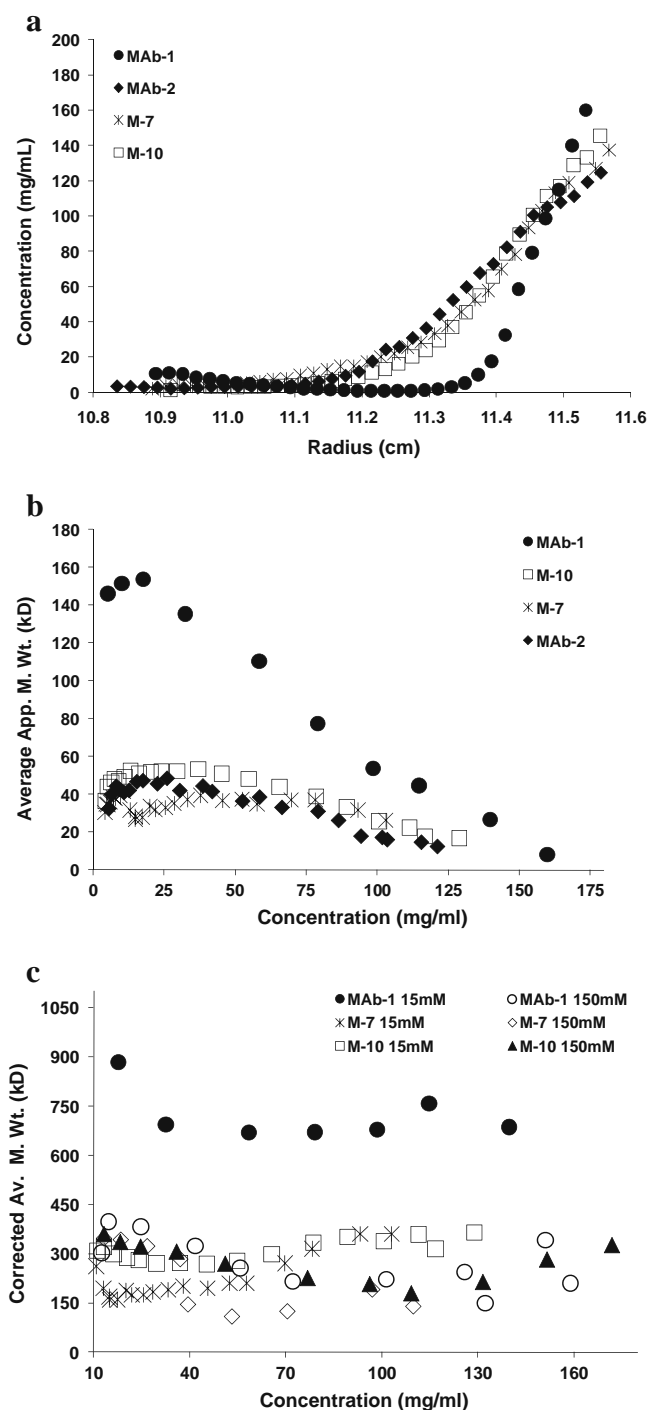
Fig. 5 The sedimentation equilibrium data for IgG$_1$ molecules (**a**), the concentration of MAbs as a function of centrifugal radial position (**b**), the apparent weight average molecular weight, M_{wapp}, of MAbs as a function of protein concentration, obtained from a sliding regression of ln(c) vs. $r^2/2$ plot from the data in figure (**a**), (**c**) the corrected weight average molecular weights (M_{wc}) for MAb1 and mutants, using the non-ideality corrections for MAb2 (Eq. 8). The measurement was conducted at pH 6.0, histidine hydrochloride buffer in 15 and 150 mM ionic strength at 12,000 rpm.

weight average molecular weight computed from a sliding regression analysis of the ln c *vs.* r^2 plot is shown in Fig. 5b, where even before any corrections for non-ideality, MAb1 appears to be more self-associated than the other MAbs. The corrected weight average molecular weights (M_{wc}) for MAb1 and mutants, using non-ideality corrections for MAb2 are shown in Fig. 5c. The M_{wc} for MAb1 is higher in comparison to M-7 and M-10, demonstrating that MAb1 undergoes self-association, whereas M-7 and M-10 do not self-associate nearly as much under these conditions. Replacing charge residues in both the variable light (VL) and the variable heavy (VH) chain in MAb1 (M-7) resulted in a lower M_{wc}, suggesting a loss in self-associating behavior. The converse case, M-10, where the VL and VH chain of MAb2 were made to look like MAb1, did not self-associate and has a viscosity-concentration profile similar to MAb2 (Fig. 5c).

Zeta Potential Measurements

Figure 6 shows the zeta potential results for IgG$_1$ molecules at solution pH 6.0, 15 mM ionic strength. The values in parentheses are the calculated charges from zeta potential results using the Poisson Boltzmann equation linearized with respect to the surface charge and zeta potential using the Debye-Hückel approximation. The zeta potential and effective charge were observed to be the lowest on MAb1 and highest for MAb2 and M-5. The average zeta potential for MAb1 at pH 6.0, 15 mM ionic strength incorporates the zeta potential measured and reported previously for MAb1, 5.01 mV in ref. (22) and 4.3±1.04 in ref. (6). The variation in measured potential essentially represents the error associated with these measurements. The M-6 net
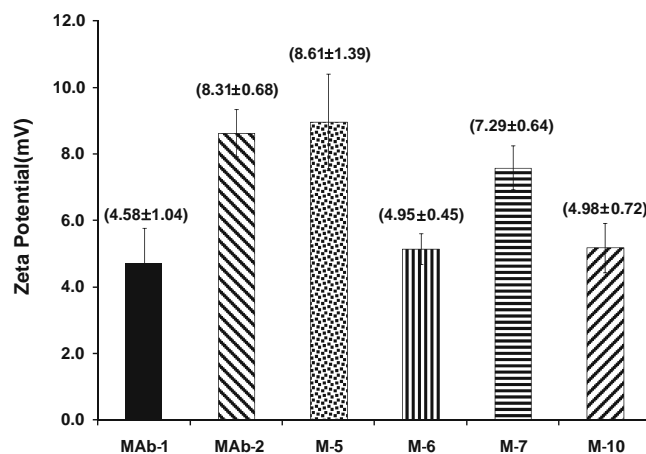

Fig. 6 Zeta potential of IgG$_1$ molecules at solution pH 6.0, 15 mM ionic strength. The measurements are performed at a concentration of 5 mg/ml at 25°C±0.1°C. The number in parentheses represents the effective charge calculated from linear correlation of ξ and Z, (Eq. 6). An average radius, $a = 5.5$ nm, determined from DLS measurements, was used for charge calculation.

charge, within error, is nearly the same as MAb-1 (Fig. 6). The swapping of charge residues in both the VL and VH chains of MAb1, i.e. M-7, resulted in an increase in surface charge and a higher zeta potential. Conversely, M-10 (on placing the charged residues in sequence of MAb2) showed a reduction in zeta potential and the effective charge (Fig. 6).

Theoretical Charge Calculations

Figure 7 shows the theoretical charges calculated for the different IgG_1 molecules as a function of pH. Table III compiles the isoelectric point (pI) for the IgG_1 molecules and the theoretical and experimental charges at pH 6.0. The isoelectric point and theoretical charge at pH 6.0 were calculated from the primary amino acid sequence (Fig. 7), whereas the experimental charges were calculated from the zeta potential measurements (Fig. 6). The experimentally measured charge for the MAbs was observed to be substantially less than the theoretically calculated one. Previously, it has been shown that the theoretically computed charge values have been in good agreement for many globular proteins (40,41), whereas for MAbs the experimental charge was observed to be 15–20 units below the theoretically estimated value (personal communication: unpublished data from the laboratory of Dr. Thomas M. Laue, University of New Hampshire). Additionally, the presence of counter-ion and its possible binding with macro-ion may alter the effective molecular charge, which is not accounted for in theoretical calculations (40). At any rate, both theoretical and experimental results indicated a change in effective charge on the molecules following mutations. The VL chain mutations in MAb1 (M-5) resulted in an increase in the pI as well as the effective charge at pH 6.0 (Table III). The replacement of histidyl
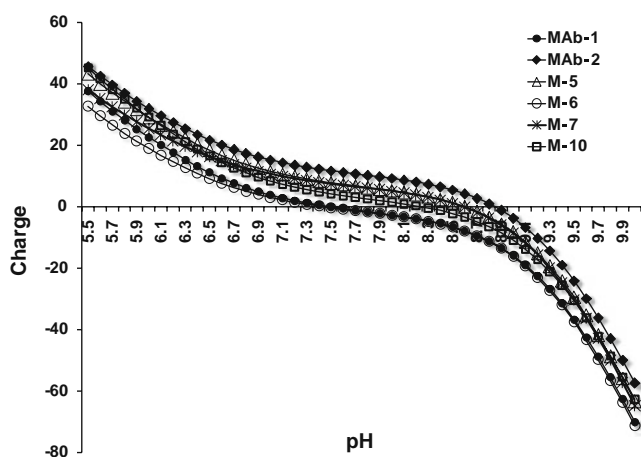
Table III Isoelectric Point (pI) and the Net Charge on IgG_1 Molecules

pH	Isoelectric Point[a]	Theoretical charge (pH 6.0)[b]	Experimental Charge (pH 6.0)[c]
MAb1	7.5	22.6	4.5 ± 1.1
M-5	8.6	29.1	8.6 ± 1.4
M-6	7.5	18.9	4.9 ± 0.4
M-7	8.6	25.4	7.3 ± 0.7
MAb2	8.8	31.9	8.3 ± 0.6
M-10	8.3	29.1	4.9 ± 0.7

[a] Calculated theoretically from the primary amino acid sequence, Fig. 7

[b] Calculated theoretically from the primary amino acid sequence at pH 6.0 (Fig. 7)

[c] From zeta potential measurements at 15 mM ionic strength (Fig. 6) using the Debye Hückel approximation with the linearized Poisson Boltzmann equation (Eq. 6)

residues in the VH chain of MAb1, M-6, did not result in a change in the pI, rather the theoretical charge at pH 6.0 was slightly less as compared with that of MAb1 (Table III). M-7 also showed a higher pI and an increase in effective charge at pH 6.0. On the other hand, M-10 indicated a slightly lower pI and less positive net charge at pH 6.0 compared with MAb2 (Table III).

DISCUSSION

Impact of Amino Acid Sequence Insert and Glycosylation on Viscosity of MAb1

Although the human Fc construct is the same for MAb1 and MAb2, the CDRs are of a different length and are essentially offset by a 4 amino acid sequence insert. M-1 was constructed so that MAb1 and MAb2 would essentially have the same length for the CDR. The results of the viscosity-concentration profile for M-1 *vs.* MAb1 show that this insert does not affect viscosity of MAb1 (Fig. 1). In addition, the profile for mutant M-11, which was made in E. coli and lacks the carbohydrate chain, is very similar to the profile for MAb-1 (Fig. 1). This is not too surprising given the limited accessibility of the carbohydrate chains in the IgG_1 structure (42). Most importantly this result suggests that the usual microheterogeneity of carbohydrate chains would be expected to have little impact on the viscosity of MAb1 and MAb2.

Protein-Protein Interactions as a Function of Concentration and pH as Detected by DLS

The k_D values determined by DLS measurements as a function of concentration provide an assessment of protein-protein interactions. In particular, a positive k_D is a result of

Fig. 7 Theoretical charge calculated on IgG_1s as function of solution pH. The charges were calculated from the primary amino acid sequence using SEDNTERP (www.bbri.org/RASMB/rasmb.html).

an increase in D_m over D_s with increasing concentration, whereas a negative k_D is a result of decreasing D_m as the solution concentration increases. Thus, a positive k_D signifies repulsive interactions, and a negative k_D implies attractive intermolecular interactions [43].

At pH 6.0, 15 mM ionic strength (Fig. 3a and Table II), MAb1 with a negative k_D suggests the presence of attractive intermolecular interactions, whereas MAb2 and mutants M-5, M-7 and M-10 interactions are overall repulsive as shown by a positive k_D. At higher ionic strength, 150 mM, the k_D value for MAb1 becomes less negative (Fig. 3a and Table II), indicating a decrease in attractive interaction. This is consistent with a recent observation which shows a negative B_{22} in MAb1 even at 600 mM solution ionic strength adjusted with NaCl [44]. The replacement of charge residues in the VL chain (M-5) resulted in complete loss of intermolecular attractions and subsequent transition to intermolecular repulsions (Table II). The replacement of charged residues in the VH chain, M-6, also resulted in loss of attractive interaction as depicted by a less negative k_D (Table II). Charge replacement in both VL and VH chains (M-7) led to a transition of intermolecular attraction to net repulsive potential between molecules (Table II). Both the effect of salt and the behavior of mutant M-5, M-6 and M-7 suggest that the charged residues in MAb1 are responsible for invoking attractive interactions in MAb1. The presence of salt results in a screening of these electrostatic interactions, either due to screening of surface charge or specific anion binding, and thereby decreases the intermolecular attractions. However, when these charge residues are replaced, as in the designed mutants, the attractive interactions are either decreased (M-6) or even completely neutralized to favor intermolecular repulsions (M-5, M-7).

MAb2 showed a positive k_D at pH 6.0 and 15 mM ionic strength, suggesting the presence of repulsive interaction between MAb2 molecules (Fig. 3a and Table II). The placement of charged residues in the sequence of MAb2 (mutant M-10) did not result in an overall attractive interaction, but rather only a slight decrease in intermolecular repulsion, as evident by a less positive k_D value (Fig. 3a and Table II). However, an increase to 150 mM ionic strength resulted in a negative k_D for MAb2, indicating the transition of overall intermolecular interactions from repulsive to attractive in nature (Fig. 3a and Table II).

Previous work (Fig. 6 in reference [22]) has shown that over a pH range from 4 to 9, the k_D value is at a minimum at pH 6 and 15 mM ionic strength. This indicates that at low ionic strength conditions, intermolecular attractions are relatively strong at pH 6 compared to other solution pHs. This is consistent with the maximum value of G′ (Fig. 6 in reference [22]) as well as the highest viscosity (Fig. 5. in ref [3]) at solution pH 6.0 [3,22]. The effect of

salt on k_D and G′ corroborated that the intermolecular interactions are electrostatic in origin [3,22].

As a function of pH, (Fig. 3b), MAb2, M-7 and M-10 showed the existence of intermolecular repulsions at pH 6.0 (positive k_D), which becomes attractive with an increase in solution pH to 9.0 (negative k_D). In comparison with mutants M-7 or M-10, MAb2 showed higher intermolecular repulsion at pH 6.0 and also higher attraction predominated at pH 8.0 or pH 9.0.

Protein-Protein Interactions as Function of Concentration and pH as Detected by High Frequency Rheometry

The solution G′ as measured by high frequency rheometry is a measure of solution rigidity that is conferred by the presence of intermolecular interactions in the system. At high concentrations the presence of attractive interactions confers relatively more rigidity to solutions, thereby restricting the molecular relaxation and momentum transfer in solution. This is reflected as a higher magnitude of solution G′ in the presence of attractive interactions as compared with intermolecular repulsions. The interrelation among pair potentials and rheological functions in establishing solution elastic modulus, G′, as a direct measure of intermolecular interaction in concentrated dispersions have been well established [45–47].

The presence of intermolecular attractions in MAb1, at pH 6.0 15 mM ionic strength, resulted in a higher solution rigidity as reflected by a high solution G′ at 125 mg/ml (Fig. 2a). Mutant M-7 did not show such high solution G′ at 125 mg/ml (Fig. 2a), which is indicative of the loss of attractive interactions and is consistent with k_D results (Fig. 3a). The solution G′ for MAb2 and mutant M-10 at 125 mg/ml was also significantly less in comparison to MAb1 due to the presence of repulsions between molecules (k_D results, Fig. 3a). M-10, in spite of the charge swap, did not show any significant change in intermolecular interactions and hence G′ as compared with MAb2 even at higher concentrations (Fig. 2a). This further supports the hypothesis that the attractive interactions between MAb1 molecules contribute to the observed concentration- dependent high viscosity, since mutant M-10 viscosity was similar to MAb2.

The pH dependence of G′ for MAb1 at 125 mg/mL at 15 mM and 150 mM ionic strength was determined previously (Fig. 6 in reference [22]). At 15 mM ionic strength, the solution G′, representative of the strength of intermolecular interactions, showed a maximum at pH 6.0. A sharp decrease in solution G′, and hence the intermolecular interactions, was observed with a change in solution pH to either an acidic or the basic side of pH 6.0 [22]. At 150 mM ionic strength the solution G′ flattens off over the

whole pH range from 4.0 to 9.0, suggesting that the intermolecular interactions were primarily electrostatic in origin and could be screened in the presence of salt (22). Although the intermolecular attractions (k_D results, Fig. 3a) and also G′ for MAb1 (Fig 2b) showed a monotonic decrease in attractive interactions with an increase in pH from 6 to 8, mutant M-7 G′ is essentially constant over the pH range from pH 6 to 7 followed by an increase from pH 7 to 8 (Fig. 2b). Due to the increase in intermolecular attractions, both MAb2 and mutant M-10 showed an increase in solution G′ with increasing solution pH, wherein solution pH 8.0 showed the highest G′ (Fig. 2b). At pH 8.0 MAb2 showed a higher G′ in comparison to mutant M-10, suggesting stronger intermolecular interaction at this pH (Fig. 2b).

The Role of Charge Residues in Invoking Specific Attractive Interactions in MAb1

Solution G′ (Fig. 2a) and k_D (Fig. 3a) indicated the presence of intermolecular attractions in MAb1 solutions. These attractive interactions resulted in self-association of MAb1 molecules at high concentrations resulting in higher M_{wc} (Fig. 5c) and high viscosity (Fig. 1). The replacement of charged residues in MAb1, either in VL (M-5) or in VH (M-6), resulted in a loss in the viscous behavior (Fig. 1). However, the viscosity of M-5 or M-6 was still higher as compared to the viscosity of MAb2 (Fig. 1), suggesting only a partial loss in self-associating behavior of MAb1. Conversely, replacing charge residues in both the VH and VL chain resulted in a decrease of viscous behavior, wherein the viscosity of M-7 was equivalent to the MAb2 solution viscosity (Fig. 1). This is in agreement with a lower M_{wc} for M-7 (Fig. 5c), signifying the loss in self-association of MAb1.

However, the substitution of charge residues in the sequence of MAb2 did not increase either the viscosity or the self-associating behavior for M-10. At pH 6.0, the M_{wc} (Fig. 5c) and the viscosity (Fig. 1) of M-10 are significantly lower as compared to MAb1 solutions.

The effect of salt on G′, k_D and M_{wc} indicates the contribution of electrostatic interactions and consequently the involvement of charge residues towards self-association and viscosity behavior of MAb1. The increase in solution ionic strength to 150 mM with NaCl resulted in a decrease in solution G′ and a less negative k_D (Fig. 3b and Table II), demonstrating a decrease in electrostatic attractive interactions. The decrease in intermolecular attractions results in a loss of self-associating behavior, which is reflected as a lower M_{wc} for MAb1 at 150 mM ionic strength (Fig. 5c). In the case of M-7, where the charge residues have been removed, the addition of salt did not make any significant change in the M_{wc}, further corroborating the role of charge residues in self-associating behavior (Fig. 5c). However, M-

10, where the charged residues are inserted in the sequence of MAb2, did not show any change in self-associating behavior at high solution ionic strengths (Fig. 5c).

At this point it may seem that the charged residues in both VL and VH chain are responsible for the self-associating behavior of MAb1, the replacement of which results in a loss of viscosity and lower M_{wc} of the M-5, M-6 and M-7 mutants. However, the behavior of M-5 and M-7 could also be explained based on the change in effective charge and pI of the molecule following mutations (Table III). Previous study on an IgG$_2$ molecule (5) and the present observations on MAb2, M-7 and M-10 (Fig. 2b) indicate that the viscosity of high concentration protein solution tends to be higher towards the pI as compared with other solution pHs. This is due to the fact that at pHs away from the pI the molecule carries a higher net charge favoring intermolecular repulsions, whereas at the pI the net molecular charge is zero, resulting in minimal repulsions. Thus, as the solution pH is shifted towards the pI, the repulsions decrease and the contribution of intermolecular attractions due to charge-charge, charge-dipole, dipole-dipole and multipole interactions increases. This is evident from the k_D data (Fig. 3b and Table II) wherein MAb2, M-7 and M-10 show intermolecular repulsions at pH 6.0. With an increase in solution pH towards the pI of these molecules, the k_D becomes negative, signifying a transition of intermolecular interactions from repulsive to attractive in nature (Fig. 3b and Table II). A further increase in pH resulted in a higher negative k_D, suggesting an increase in attractive intermolecular interactions (Fig. 3b). The increase in intermolecular attractions results in an increase in viscosity (data not shown) and solution G′ towards the pI (Fig. 2b).

The mutations in the VL and VH chain, M-7, resulted in an increase in effective charge on the molecule (Fig. 6). This increase in net molecular charge would favor intermolecular repulsions. This is corroborated by the solution G′ (Fig. 2a) and k_D (Fig. 3a) measurements, indicating the presence of repulsive interactions in M-7 solutions. The presence of repulsions does not favor the self-association, resulting in a lower M_{wc} (Fig. 5c) and loss of solution viscosity (Fig. 1) for M-7. A similar argument would hold for the behavior of M-5, wherein the mutations are made only in the VL chain, resulting in an increase in pI and the effective charge (Table III). This increase in net molecular charge will lead to an increase in intermolecular repulsions (k_D results, Table II), resulting in lower viscosity as observed (Fig. 1). The increase in net molecular charge and repulsive interactions therefore explains the loss in viscosity and self-association for M-5 and M-7.

However, the behavior of M-6, wherein the mutations are made only in the VH chain, supports our previous hypothesis that the specific attractive interactions originate

from a number of histidyl residues in the CDR (22). The replacement of these charged histidyl residues in MAb1, i.e. the charge-swap mutant M-6, did not result in an increase in the pI or the net charge of the molecule (Table III). In fact, the theoretical calculations (Fig. 7) showed slightly lower net charge for M-6 as compared with MAb1, and the experimental charge is nearly the same (Fig. 6). In spite of this, M-6 showed a lower viscosity as compared with MAb1 (Fig. 1). This loss in viscosity cannot be attributed to an increase in intermolecular repulsions, since the net charge remains the same. If only the net charge were governing the solution behavior and the intermolecular interactions, then the viscosity of M-6 should have been equivalent to MAb1. This indicates that the histidyl residues are responsible for the high viscosity of MAb1. Although at this point we have not quantified molecular dipoles, we hypothesize that the replacement of positively charged histidyl residues essentially results in a loss of net molecular dipole, thereby decreasing the electrostatic attractive interactions and loss of self-association. However, the attractions are not completely lost after swapping in the histidyl residues, as M-6 still exhibits a negative k_D, although lesser in magnitude as compared with MAb1 (Table II). Thus, it appears that there are other factors, in addition to the charged histidyl residues, that contribute towards the intermolecular attraction in MAb-1 at pH 6.0, and will be elucidated further.

The behavior of mutant M-10 can also be explained on the basis of net positive molecular charge (Table III). In low ionic strength solutions, both MAb2 and M-10 showed a positive k_D, indicating the presence of repulsive interactions at pH 6.0 (Fig. 3(a)). The k_D value for M-10 is lower as compared to MAb2, suggesting that the placement of charge residues did result in some attraction between molecules, thereby decreasing intermolecular repulsions. However, the net intermolecular interactions are still repulsive, and therefore do not favor self-association (Fig. 5c) or an increase in viscosity (Fig. 1). This is evident even at 125 mg/ml, where the solution G' for M-10, though slightly less, is not very different as compared to MAb2, suggesting similar magnitude of intermolecular interactions in the two molecules (Fig. 2a). Although the addition of salt decreases the repulsive interactions to the extent of favoring intermolecular attractions, resulting in negative a k_D for MAb2 (Fig. 3a), the insertion of the charged residues is not able to produce the same effect.

It needs to be emphasized that the behavior of MAb1 is very unique. The theoretical and measured pI (using isoelectric focusing) of MAb1 is ~7.5. However, it shows a high viscosity and solution G' at pH 6.0 (3,22), which is about 1.5 units away from the pI. Moreover, attractive interactions persist in MAb1 solutions despite it being positively charged at pH 6.0 (Figs. 3a and 6), also previously published by Yadav et al. (22). The behavior of MAb1,

therefore, cannot be explained on the basis of nonspecific electrostatic repulsive or attractive intermolecular interactions as a function of pH. The origin of these attractive interactions is localized specifically in the Fab regions of MAb1 due to the presence of a number of charged residues (21,22). The conformational state of these residues will be critical in regulating the specific attractive interaction and complementary molecular alignment that results in self-association. At this stage it would be hard to justify whether the conformational state of histidyl residues upon insertion in the sequence of MAb2 is the same as that of MAb1. This is evident from comparison of the CD spectra of the MAb2 and M-10 (Fig. 4(b)), which suggests that the local environment around residues may be slightly different. Therefore, the placement of these residues in a different IgG$_1$ molecule may not result in similar interactions that persist in MAb1 solutions, which, in part, may also explain why the insertion of charged residues did not result in an increase in viscosity of M-10.

SUMMARY AND CONCLUSIONS

Several previous studies on MAb1 have suggested the role of electrostatic interactions in governing the self-associating behavior at high concentrations (3,6,21,22). The self-association appears to originate from the Fab regions (21, 22). Although MAb1 and MAb2 have been constructed with essentially the same human Fc framework and the differences reside only in the CDR and flanking amino acid residues, MAb1 shows significant self-association and high viscosity at pH 6.0, whereas MAb2 is less viscous accompanied by a lower degree of self-association (44). A comparison of the amino acid sequence in the CDR showed the presence of several charge residues in both VL (aspartate, glutamate and histidyl) and VH (several histidyl residues) chains. The analysis of MAb1, MAb2 and the designed mutants seems to point towards the involvement of these residues in governing the solution behavior of MAb1 at high concentrations. The attractions that result from the specific residues are hypothesized to result in an extensive organization, or clustering, of molecules in solution at high concentration. Essentially, the movement of one molecule would then result in an application of force on other molecules, which may result in a viscous drag yielding higher viscosities as concentration is increased. The hypothesis of the existence of such network attractions is controversial, but has been proposed based on several experimental approaches (48–52). Nevertheless, the present study provides experimental evidence that the presence of exposed charged residues in the CDR of MAb1 are critical in determining the self-associating and highly viscous behavior observed at pH 6.0. The replacement of these

charge residues results in a loss of self-associating behavior, which in turn results in lower viscosities in high concentration solutions.

ACKNOWLEDGMENTS

REFERENCES

1. Sharma VK, Chih HW, Mrsny RJ, Daugherty AL. The formulation and delivery of monoclonal antibodies. In: Zhiqiang A, editor. Therapeutic monoclonal antibodies: from bench to clinic. New Jersey: John Wiley and Sons; 2009. p. 675–710.
2. Shire SJ, Zahra S, Liu J. Challenges in the development of high protein concentration formulation. In: Shire SJ, Gombotz WR, Peters KB, Andya JD, editors. Current trends in monoclonal antibody development and manufacturing. New York: Springer; 2010. p. 131–40.
3. Liu J, Nguyen MDH, Andya JD, Shire SJ. Reversible self-association increases the viscosity of a concentrated monoclonal antibody in aqueous solution. J Pharm Sci. 2005;94:1928–40.
4. Salinas BA, Sathish HA, Bishop SM, Harn N, Carpenter JF, Randolph TW. Understanding and modulating opalescence and viscosity in a monoclonal antibody formulation. J Pharm Sci. 2009;99:82–93.
5. Saluja A, Badkar AV, Zeng DL, Nema S, Kalonia DS. Application of high-frequency rheology measurements for analyzing protein-protein interactions in high protein concentration solutions using a model monoclonal antibody (IgG$_2$). J Pharm Sci. 2006;95:1967–83.
6. Yadav S, Shire SJ, Kalonia DS. Factors affecting the viscosity in high concentration solutions of different monoclonal antibodies. J Pharm Sci. 2010;99:4812–29.
7. Daugherty AL, Mrsny RJ. Formulation and delivery issues for monoclonal antibody therapeutics. In: Shire SJ, Gombotz WR, Peters KB, Andya JD, editors. Current trends in monoclonal antibody development and manufacturing. New York: Springer; 2010. p. 103–30.
8. Minton AP. Implications of macromolecular crowding for protein assembly. Curr Opin Struct Biol. 2000;10:34–9.
9. Minton AP. Influence of macromolecular crowding upon the stability and state of association of proteins: predictions and observations. J Pharm Sci. 2005;94:1668–75.
10. Saluja A, Badkar AV, Zeng DL, Kalonia DS. Ultrasonic rheology of a monoclonal antibody (IgG$_2$) solution: implications for physical stability of proteins in high concentration formulations. J Pharm Sci. 2007;96:3181–95.
11. Andya JD, Hsu CC, Shire SJ. Mechanisms of aggregate formation and carbohydrate excipient stabilization of lyophilized humanized monoclonal antibody formulations. Pharm Sci. 2003;5:E10.
12. Creed D. The photophysics and photochemistry of the near-UV absorbing amino acids. II. Tyrosine and its simple derivatives. Photochem Photobiol. 1984;39:563–75.
13. Chi EY, Krishnan S, Randolph TW, Carpenter JF. Physical stability of proteins in aqueous solution: mechanism and driving forces in nonnative protein aggregation. Pharm Res. 2003;20:1325–36.
14. Fernandez A. What factor drives the fibrillogenic association of β-sheets? FEBS Lett. 2005;579:6635–40.
15. Braun A, Kwee L, Labow MA, Alsenz J. Protein aggregates seem to play a key role among the parameters influencing the antigenicity of interferon alpha (IFN-α) in normal and transgenic mice. Pharm Res. 1997;14:1472–8.
16. Cleland JL, Powell MF, Shire SJ. The development of stable protein formulations: a close look at protein aggregation, deamidation, and oxidation. Crit Rev Ther Drug. 1993;10:307–77.
17. Koren E, Zuckerman LA, Mire-Sluis AR. Immune responses to therapeutic proteins in humans - clinical significance, assessment and prediction. Curr Pharm Biotechnol. 2002;3:349–60.
18. Thornton CA, Ballow M. Safety of intravenous immunoglobulin. Arch Neurol. 1993;50:135–6.
19. Shire SJ, Shahrokh Z, Liu J. Challenges in the development of high protein concentration formulations. J Pharm Sci. 2004;93:1390–402.
20. Cromwell MEM, Hilario E, Jacobson F. Protein aggregation and bioprocessing. AAPS J. 2006;8:E572–9.
21. Kanai S, Liu J, Patapoff TW, Shire SJ. Reversible self-association of a concentrated monoclonal antibody solution mediated by Fab-Fab interaction that impacts solution viscosity. J Pharm Sci. 2008;97:4219–27.
22. Yadav S, Liu J, Shire SJ, Kalonia DS. Specific interactions in high concentration antibody solutions resulting in high viscosity. J Pharm Sci. 2010;99:1152–68.
23. Jefferis R. Glycosylation of recombinant antibody therapeutics. Biotechnol Prog. 2005;21:11–6.
24. Minton AP. Analytical centrifugation with preparative ultra-centrifuges. Anal Biochem. 1989;176:209–16.
25. Pollet RJ, Haase BA, Standaert ML. Macromolecular characterization by sedimentation equilibrium in the preparative ultracentrifuge. J Biol Chem. 1979;254:30–3.
26. Minton AP. The effect of volume occupancy upon the thermodynamic activity of proteins: some biochemical consequences. Mol Cell Biochem. 1983;55:119–40.
27. Chatelier RC, Minton AP. Sedimentation equilibrium in macromolecular solutions of arbitrary concentration. II. Two protein components. Biopolymers. 1987;26:1097–113.
28. Chatelier RC, Minton AP. Sedimentation equilibrium in macromolecular solutions of arbitrary concentration. I. Self-associating proteins. Biopolymers. 1987;26:507–24.
29. Tanford C. Thermodynamics. In: Tanford C, editor. Physical chemistry of macromolecules. New York: John Wiley & Sons; 1961. p. 180–272.
30. Roark DE, Yphantis DA. Equilibrium centrifugation of nonideal systems. The donnan effect in self-associating systems. Biochemistry. 1971;10:3241–9.
31. Saluja A, Kalonia DS. Measurement of fluid viscosity at microliter volumes using quartz impedance analysis. AAPS PharmSciTech. 2004;5:68–81.
32. Bund A, Schwitzgebel G. Viscoelastic properties of low-viscosity liquids studied with thickness-shear mode resonators. Anal Chem. 1998;70:2584–8.
33. Hunter RJ. The Calculation of Zeta Potential. In: Ottewill RH and Rowell RL, editors. Zeta Potential in Colloid Science Principles and Applications. New York: Academic; 1981. p. 59–124.
34. Delgado AV, Gonzalez-Caballero F, Hunter RJ, Koopal LK, Lyklema J. Measurement and interpretation of electrokinetic phenomena. J Colloid Interface Sci. 2007;309:194–224.
35. Hunter RJ. Charge and potential distribution at interface. In: Ottewill RH and Rowell RL, editors. Zeta potential in colloid science principles and application. New York: Academic; 1981. p. 11–58.
36. Durant JA, Chen C, Laue TM, Moody TP, Allison SA. Use of T4 lysozyme charge mutants to examine electrophoretic models. Biophys Chem. 2002;101–102:593–609.

37. Moody TP, Shepard HK. Nonequilibrium thermodynamics of membrane-confined electrophoresis. Biophys Chem. 2004;108:51–76.

38. Brown W, Nicolai T. Dynamic light scattering: the method and some applications. New York: Oxford University Press; 1993.

39. Teraoka I. Polymer solutions: an introduction to physical properties. New York: Wiley; 2002.

40. Moody TP, Kingsbury JS, Durant JA, Wilson TJ, Chase SF, Laue TM. Valence and anion binding of bovine ribonuclease A between pH 6 and 8. Anal Biochem. 2005;336:243–52.

41. Schellman JA, Stigter D. Electrical double layer, zeta potential, and electrophoretic charge of double-stranded DNA. Biopolymers. 1977;16:1415–34.

42. Wang W, Singh S, Zeng DL, King K, Nema S. Antibody structure, instability, and formulation. J Pharm Sci. 2007;96:1–26.

43. Li S, Xing D, Li J. Dynamic light scattering application to study protein interactions in electrolyte solutions. J Biol Phys. 2004;30:313–24.

44. Scherer TM, Liu J, Shire SJ, Minton AP. Intermolecular interactions of IgG1 monoclonal antibodies at high concentrations characterized by light scattering. J Phys Chem B. 2010;114:12948–12957.

45. Buscall R, Goodwin JW, Hawkins MW, Ottewill RH. Viscoelastic properties of concentrated latices: part 1. - methods of examination. J Chem Soc, Faraday Trans 1 F. 1982;78:2873–87.

46. Buscall R, Goodwin JW, Hawkins MW, Ottewill RH. Viscoelastic properties of concentrated latices: part 2. - Theoretical analysis. J Chem Soc, Faraday Trans 1 F. 1982;78:2889–99.

47. Kriegerand IM, Eguiluz M. Second electroviscous effect in polymer latices. Trans Soc Rheol. 1976;20:29–45.

48. Porcar L, Falus P, Chen WR, Faraone A, Fratini E, Hong K, *et al.* Formation of the dynamic clusters in concentrated Lysozyme protein solutions. J Phys Chem Lett. 2010;1:126–9.

49. Shukla A, Mylonas E, Di Cola E, Finet S, Timmins P, Narayanan T, *et al.* Absence of equilibrium cluster phase in concentrated lysozyme solutions. Proc Nat Acad Sci. 2008;105:5075–80.

50. Shukla A, Mylonas E, Di Cola E, Finet S, Timmins P, Narayanan T, Svergun DI. Reply to Stradner *et al.*: equilibrium clusters are absent in concentrated lysozyme solutions. Proc Nat Acad Sci. 2008;105,E76.

51. Stadler AM, Schweins R, Zaccai G, Lindner P. Observation of a large-scale superstructure in concentrated hemoglobin solutions by using small angle neutron scattering. J Phys Chem Lett. 2010;1:1805–8.

52. Stradner A, Sedgwick H, Cardinaux F, Poon WCK, Egelhaaf SU, Schurtenberger P. Equilibrium cluster formation in concentrated protein solutions and colloids. Nature. 2004;432:492–5.